Boiling & Condensation 2015

9th International Conference on Boiling and Condensation Heat Transfer
April 26-30, 2015 – Boulder, Colorado

A CRITICAL REVIEW ON THE MECHANISMS TRIGGERING THE DNB IN SUBCOOLED FLOW BOILING USING A COMPLEMENTARY EXPERIMENTAL APPROACH

Gregor Bloch*, Moritz Bruder, Thomas Sattelmayer
*Author for correspondence
Lehrstuhl für Thermodynamik
Technische Universität München
Boltzmannstraße 15
85748 Garching bei München
Email: gbloch@mytum.de

Abstract

New experimental observations on the trigger mechanisms for the depature from nucleate boiling in subcooled flow boiling are presented. A critical review of available mechanistic models and trigger mechanisms is given and a comparison to the experimental results is presented. Experimental results are derived using a matrix of complementary measuring techniques to review the validity of the proposed mechanisms for upflow boiling of Novec 649 in a vertical, rectangular channel with an inner diameter of 40 mm. Mass fluxes are in the range of $1000\,\mathrm{kg\,m^{-2}s^{-1}}$ and subcoolings range from 27 to 9 K. Using the experimental data, new insight is provided with regard to the available models and possible CHF triggers. A conceptualization for a refined phenomenological modeling approach is presented, and possible future research discussed.

1 Introduction

The departure from nucleate boiling (DNB) is one of the most relevant phenomena in boiling heat transfer. A large number of correlations and models have been presented over the last decades, however the opinion on the actual trigger events of the transition is still divided. This can be attributed to the difficulties in experimentally accessing the relevant effects, as this requires analysis on a range of time and geometrical scales for several orders of magnitude each (from µm to m, and from µs to minutes), taking place in a highly complex multiphase flow. Still, many current models have been developed based mainly on photographic visualization studies, which have greatly helped in understanding the general vapor behavior but cannot yield information on a number of parameters deemed crucial in understanding the DNB transition. Accordingly, the mechanisms presented in many models lack actual experimental confirmation. To overcome this shortage, an approach was made using a matrix of five measuring techniques complementing each other in order to gain enhanced insight into phenomena in both the vapor and liquid phase, as well as heat transfer effects in the heater and the liquid phase and local properties in the high quality region close to the heater.

2 Current mechanistic CHF models

To improve calculation of the critical heat flux over empirical models, so called phenomenological or mechanistic models have been developed based on physical mechanisms leading up to the CHF. These types of models offer a potentially higher validity than purely empiririal ones, provided the correct definition of the mechanisms. These models have so far mainly seen use in academia, while for industrial applications the use of empirical correlations is still favored (Weisman, 1996). However, a correct phenomenological description of the actual trigger mechanisms for CHF may not only improve the accuracy of calculations but also help in defining measures to prevent or postpone the departure from nucleate boiling. Furthermore, the understanding of CHF trigger mechanisms is of utmost importance also for a correct formulation of CFD models. Up to now, CFD modeling of CHF is still mainly based on available empirical correlations and blending modeling setting CHF at predefined void fractions (Krepper and Rzehak, 2011; Lifante et al., 2013). In the following paragraph, the three most recently used types of mechanistic models shall be presented and discussed. These are namely the *bubble crowding model*, the *sublayer dryout model* and the *interfacial lift-off model*.

2.1 Near wall bubble crowding model

The *near wall bubble crowding* assumes the loss of quenching and subsequent CHF to be caused by a rising concentration of vapor bubbles near the heater surface, which prohibits turbulence in the bulk flow from penetrating the vapor layer and transport

fresh liquid to the heater surface. It is assumed that this happens at a critical vapor fraction in the vapor layer, which is derived from a geometrical balance of given bubbles, that begin to coalesce after reaching the critical vapor fraction. The mechanism was first proposed by Weisman and Pei (1983), based on previous work by Hebel et al. (Hebel et al., 1981), (Hebel and Detavernier, 1982). The original model assumed homogeneous flow of vapor bubbles and liquid within the bubbly layer. Ying and Weisman (1986) expanded the model to lower mass velocities, replacing the homogeneous flow with a slip model taking into consideration the buoyancy effects of larger bubbles. Lim and Weisman (1990) also applied the model to flow in channels with partial heating, while Yang and Weisman (1991) further expanded the model for calculation of pre-CHF heat fluxes throughout the detached bubble region. The model was based mainly on a small number of visualization studies.

2.2 Sublayer dryout model

The *sublayer dryout model*, first introduced by Lee and Mudawar (1988) based on an older model with similar mechanism by Haramura and Katto (1983), has received increased attention over the last twenty years (Katto, 1990a,b; Celata et al., 1994, 1995). According to this model, CHF occurs when a liquid sublayer present under the vapor bubbles during nucleate boiling cannot be replenished from the bulk flow any more and evaporates, creating a dry spot on the heater surface. To overcome some inconsistencies of the original sublayer dryout model, Celata et al. (1999) developed the *superheated layer vapor replenishment model*, which assumes a liquid layer at saturation temperature (superheated layer) close to the heater surface, that dries out at CHF and is replenished by a vapor blanket. The model was mainly developed for high mass fluxes and liquid subcoolings. Since a main assumption is an isolated layer of liquid close to the heater surface as the only possible position for vapor bubbles, the authors state a loss of validity when local thermodynamic conditions at CHF approach the saturated state of the liquid bulk (Celata et al., 1999). The model basics have mainly been developed from visualization studies on small scale experiments, such as the falling film evaporation study by Mudawwar et al. (1987). Experimental validation for the model on larger scale boiling experiments is scarce, mainly because the postulated thin sublayer is challenging to access with available measuring techniques.

2.3 Interfacial Lift-Off model

Another very recent model is the *interfacial lift-off model*. In sharp contrast to the sublayer dryout model, this model focuses on the global behaviour of the vapor rather than local microscopic effects. Here, a periodic behaviour of the vapor layer along the whole heated length is postulated, with waves of higher void fractions alternating with areas where liquid can access the heater. At the DNB, these areas are assumed to lift-off from the heater surface, leading to liquid blockage and subsequent CHF. The model was first proposed by Galloway and Mudawar (1993a,b), based on photographic studies in a rectangular channel of 1.6x6.4 mm^2 with a copper heater and FC87 as boiling fluid. Galloway and Mudawar (1993a) defined three different regimes to be observed from ONB up to CHF. In the *discrete bubble regime* up to 40 % of CHF, isolated bubbles were observed, while in the *coalescent bubble regime* at up to 60 % of CHF coalescence and formation of larger bubbles were observed. This led to the final *wavy liquid-vapor layer*, where all bubbles were observed to coalesce into a continuous wavy vapor layer periodically touching the heater surface. Vapor wavelengths were reported in the range of 3 to 6 mm with amplitudes of 0.7 to 1.8 mm. Zhang et al. (2002, 2004a) later conducted experiments with different orientation of the heater surface relative to gravity which revealed more flow regimes. For vertical upflow however, the three aforementionend regimes were confirmed. The areas where the vapor layer touched the heater surface and thereby allowed for access of liquid where denoted as *wetting fronts*. These were assumed to be the main mechanism of heat transfer in the wavy vapor layer regime. At CHF, the wetting front at the leading edge of the heater was observed to be lifted off from the heater surface, caused by a vigorous effusion of vapor beneath the front (Galloway and Mudawar, 1993a). This led to further increases in heater temperature, culminating in the departure from nucleate boiling. Figure 1 shows a comparison of the main mechanisms for the three discussed models.

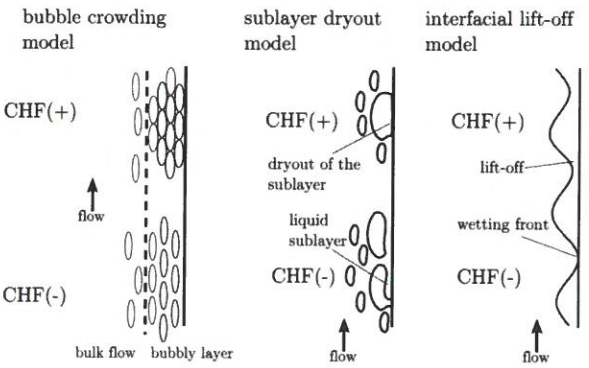

Figure 1. Main trigger mechanisms for the CHF transition from the different mechanistic models (adapted from Konishi et al. (2013)).

2.4 Overview

As of today, it still remains unclear which of the discussed models best represents the actual CHF trigger mechanism. This is mainly due to the challenging experimental approach, and also the wide range of phenomena observed in the field, which range from regimes similar to pool boiling at low subcoolings and mass fluxes up to extreme low quality boiling at high subcoolings and mass fluxes. This leaves the question of whether one mechanism might even be enough to describe DNB sufficiently. Also, as Tong and Weisman (1996), (Weisman, 1996) pointed out, several models may be correct due to imprecise definition of the actual CHF event itself: while the bubble crowding model focuses on the behavior of the global vapor layer shortly before CHF, the sublayer dryout models focuses on local sublayer behavior at or even slightly after CHF.

3 Experimental approach

An approach using an array of complementing measuring techniques is used to gain enhanced insight into the boiling processes at CHF. The main boiling rig consists of a flow loop with a vertically orientated, rectangular boiling chamber. The basic layout of the setup is given in Figure 2. High-speed photography is applied to provide general information about the geometry and velocity

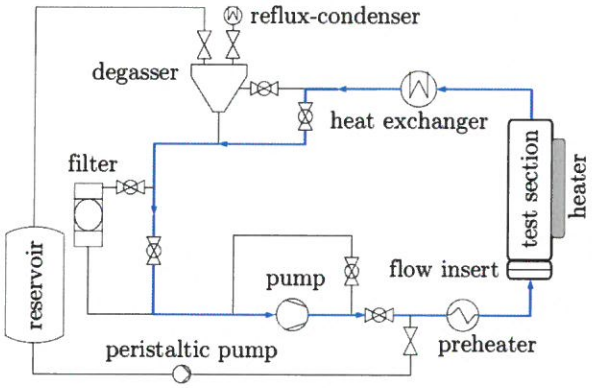

Figure 2. Schematic of the flow loop.

of the overall vapor phase. These results are complemented with PIV measurements to give insight into the behavior of the bulk liquid phase around the vapor layer. To give information about the temperature distribution, shadowgraphy and digital holographic interferometry are used (Bloch et al., 2014). Lastly, three optical probes with a diameter 200 µm of are used to give point wise information on the behavior of the vapor layer close to the heater surface in areas not accessible to the other techniques. Figure 3 shows the general layout of the test rig with the applied measuring techniques. The main boiling chamber is of square inner shape

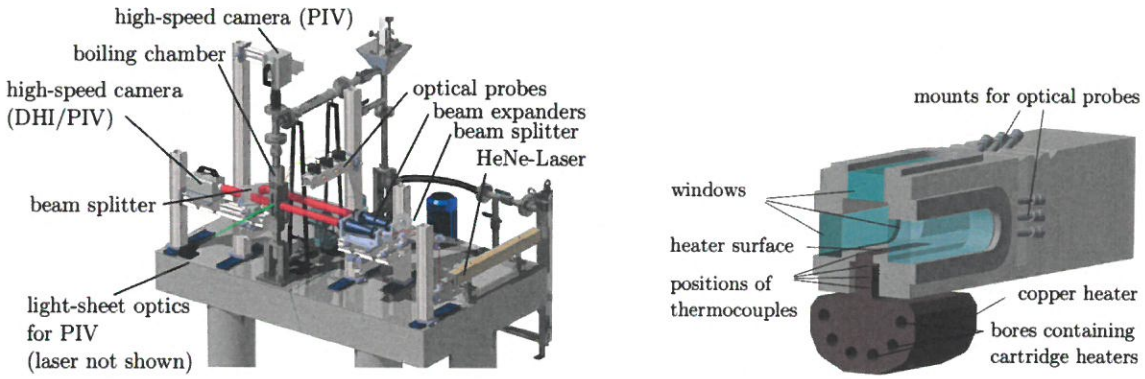

Figure 3. Left: CAD-drawing of the test rig showing the setup of the holographic interferometry together with the optical probes and PIV in vertical orientation (note that holography and PIV are not applied simultaneously in the experiments). Right: sectional view of the main boiling chamber (rotated by 90 deg).

with dimensions of 40x40 mm^2 and a total length of 500 mm. A copper heater mounted flush into one of the channel walls is used for heating, see Figure 3. The heated area inside the chamber has a total length of 200 mm and a width of 15 mm. The leading edge of the heater is positioned 75 mm above the inlet. Three rows of thermocouples are installed along the length of the heater at distances of 50, 100 and 150 mm to the leading edge of the heater, each row consisting of four thermocouples at distances of 1 to

13 mm from the heater surfaces. From the temperature gradient between the thermocouples, heat fluxes are calculated and surface temperature is extrapolated. Further thermocouples are positioned in the liquid phase to measure in- and outlet temperatures of the fluid. At the entrance to the boiling chamber, flow inserts can be placed to create turbulence and secondary flows. Used inserts include delta wings (Bloch et al., 2012), twisted tapes and perforated plates (Bloch and Sattelmayer, 2014). In the experiments discussed here, only the effects of an orifice with a single 25 mm-diameter hole are discussed. The applied measuring techniques are only shortly described here for brevity. High-speed photography and shadowgraphy were applied using a Photron Fastcam SA5 high-speed camera as described in (Bloch et al., 2013a) using a back-lit setup. Recording rates were typically at 2000 fps for the images shown here. Various in-house algorithms were implemented to derive statistical evaluations of vapor distributions, velocities, and periodic behavior in both steady state and transient measurements. Digital holographic interferometry, as discussed in detail in (Bloch et al., 2014), was done using an in-line holographic setup with separated beams as shown in Figure 3. A He-Ne laser was used for illumination, while the same SA5 camera as for the photography was used (without lens). PIV was done both in cold flow to define the flow characteristics (Bloch et al., 2012) as well as in nucleate and film boiling (Bloch et al., 2013a). A time averaged setup was used for the flow characterisation, while a high-speed approach was used for the boiling studies. The optical probes consisted of 200 µm silica fibres, the tips of which were polished conically using an in-house setup as discussed in Bloch et al. (2013b). The probes are illuminated by a diode laser and detect changes in the refractive index at the tips, which is measured using beam splitter optics. The experiments were mainly conducted in steady state boiling at CHF(-), an operating point which was defined as having a surface superheat 1 K below the temperature at which CHF was observed to occur for the given parameters. In addition to this, transient measurements ranging from the onset of nucleate boiling over the CHF transient and well into film boiling were also conducted to study the actual DNB process.

4 Experimental results

At first, a summary of general observations on the boiling system shall be given to provide an overview of the main effects that were observed. Following this, specific effects relating to the trigger mechanisms given by available models are discussed separately.

4.1 Vapor structure and movement

Figure 4 shows the observed vapor structure at a liquid subcooling of 9 K over a larger area (above) and in detail (below). It could be observed that the vapor behaviour was highly periodic, with larger agglomerations appearing at roughly constant frequencies of approx. 25 Hz (Bloch et al., 2013a). In the wakes of these agglomerations, movement of fresh liquid towards the heater surface could be visualized using PIV as shown in (Bloch et al., 2013a). Below the coalesced vapor structure, single

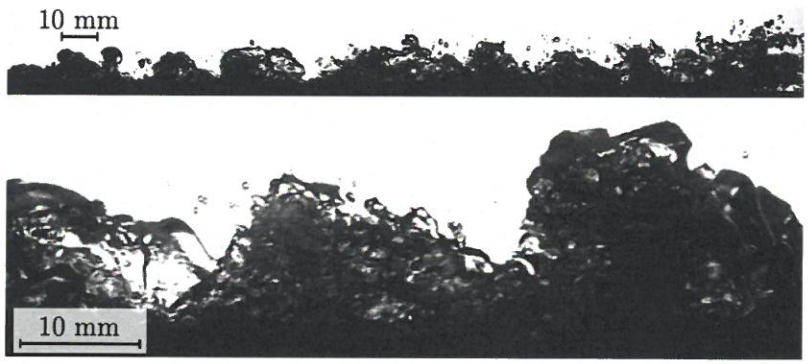

Figure 4. Vapor structure over a larger area (above) and in detailed recording of the middle section (below), both for fully developed nucleate boiling at inlet subcooling of 9 K and flow superficial velocity of 0.6 m/s (images not synchronous). The images are rotated by 90 degrees, i.e. the inlet is on the left side.

vapor bubbles could be observed as well, moving at high velocities. This was in accordance with the results of e.g. (Bang et al., 2004; Jiji, 1962), who also reported a bubbly layer underneath a layer of vapor clots. The distribution of the vapor phase over the channel cross section is of particular interest with regard to the phenomena causing the departure from nucleate boiling. Therefore, measurements were conducted for steady-state boiling at wall superheats of 1 K below the value where CHF occured for the given parameters. This state was defined as CHF(-). Experiments were conducted using both high-speed photography and optical probes. The upper plot in Figure 5 shows a statistical analysis of the void distribution as averaged intensity per pixel column for a total of 17.000 images recorded at 2 kHz. The heater surface is at the right hand side of the plot at 40 mm. To determine the velocity of the continuous vapor phase near the heater surface, a cross-correlation algorithm was applied on the high-speed photography images. Figure 5 (bottom) shows the resulting velocity distributions for subcoolings of 9, 14 and 19 K. It could be shown that the velocity assumes an initial value close to the superficial velocity (0.6 m/s) in areas of low gas holdup, and increases linearly in the region of higher holdups towards the heater surface. The maximum values were observed at distances of 2-4 mm to the heater surface,

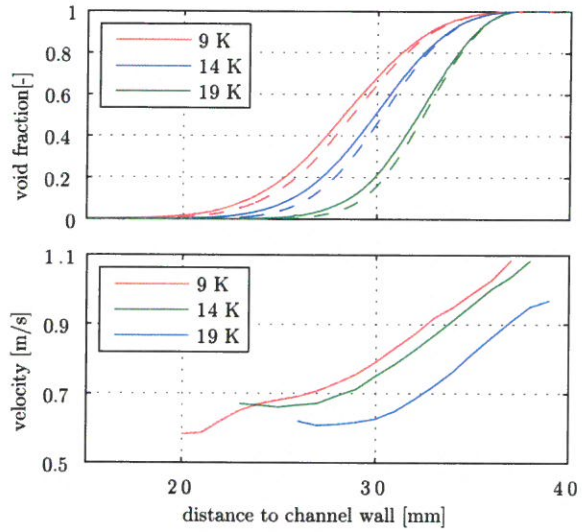

Figure 5. HS photography: Distribution of vapor phase and velocity profiles from cross correlation, plotted over the channel cross section for different subcoolings (heater surface is at the right hand side at 40 mm, v_s=0.6 m/s). Dashed lines indicate the void fraction after removal of isolated bubbles. From (Bloch et al., 2013a).

with values ranging up to 1.1 m/s. Measurements closer to the heater surface were not possible with the photographic method due to high vapor concentration. The observed increase in velocity could be attributed to buoyancy effects brought about by the high vapor concentration close to the heater. More detailed measurements on the vapor distribution close to the heater surface obtained with optical probes are given in the following paragraphs.

4.2 Heat transfer

To study the temperature distribution in the boiling flow, simple shadowgraphy was used to give a general visualization of strong temperature gradients, while for a more precise investigation digital holographic interferometry was used as given in (Bloch et al., 2014). Figure 6 shows shadowgrams of a boiling flow at CHF(-) for a fluid subcooling of 27 K. It can be observed that a layer of heated liquid is present above the vapor with a thickness of approx. 5-10 mm. Figure 7 shows DHI results. It could be shown

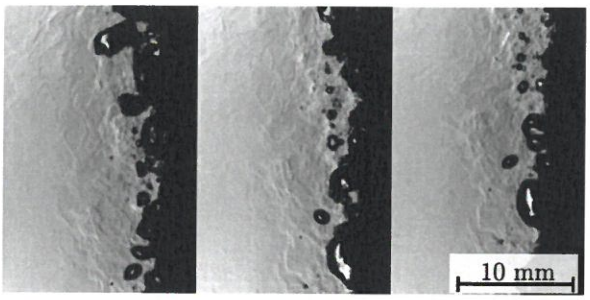

Figure 6. Shadowgrams for flow boiling CHF at 27 K subcooling. A layer of heated liquid can be observed above the vapor bubbles. (v_s=0.6 m/s).

that in the liquid areas between vapor agglomerations, the liquid is of approximately the same temperature as in the liquid layer above the agglomerations seen from the shadowgraphy. Considering significant transport towards the heated surface in wakes of agglomerations that was measured by PIV (Bloch et al., 2013a), this indicates an important quenching mechanism.

5 Comparison of results to available DNB-trigger mechanisms suggested by mechanistic models

In the following section, CHF trigger mechanisms proposed by the mechanistic models discussed in the previous section are critically reviewed with reference to the experimental results received from the applied experimental approach. For this, the main model assumptions are recapitulated and compared to the experimental results. A complete derivation of the models is not given for reasons of brevity, the aim of the model description is rather to point out the main effects accessible with experimental methods.

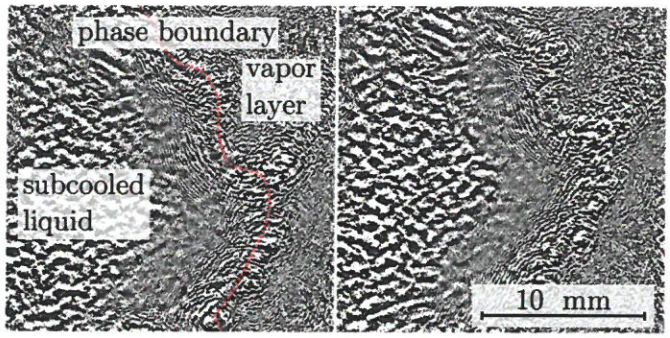

Figure 7. Holographic interference phase map showing area of lower vapor quality between two agglomerations and the surrounding liquid phase. (T_{sub}=5 K, v_s=0.6 m/s).

5.1 Bubble crowding model: critical evaluation

As turbulent interchange is one of the main parameters within the bubble crowding model, experiments were conducted on the actual influence of the turbulent flow on the vapor interface and the critical heat flux. For this, boiling experiments were conducted with varying degrees of turbulence and secondary flows using an orifice placed at the inlet of the boiling chamber. Fig. 8 shows a photograph of the vapor structure for boiling with the orifice at the inlet. It was observed that the increasing turbulence lead to a better distribution of the vapor and therefore to a thinner vapor layer in the proximity of the heater surface. Studying this

Figure 8. Vapor Structure at CHF(-) for with an orifice insert for a subcooling of 9 K and v_s=0.6 m/s (image rotated by 90°). The flow without inserts is shown above in Figure 4.

influence statistically at different fluid subcoolings yielded the results shown in fig. 9. The figure shows the averaged intensity per pixel column for a total of 17,000 images for each curve. It could be observed that the penetration depth of turbulence regarding the vapor, i.e. the difference in vapor layer thickness was roughly constant for the orifice at the studied subcoolings. Taking the difference at 90 % void fraction, a reduction of 1.2, 1.3 and 1.5 mm in thickness was observed at subcoolings of 9, 14 and 19 K respectively. This was equivalent to 17, 21 and 31 relative reduction. Comparing this to the observed increases in CHF yielded good agreement, as CHF increase was observed at 19, 23 and 25 % for subcoolings of 9, 14 and 19 K respectively (Bloch and Sattelmayer, 2014). While this does not fully confirm the assumptions of the model concerning a linear influence of turbulence intensity , it does confirm that there appears to be a critical vapor thickness for given thermohydraulic parameters, the reduction of which results in an increase in CHF equivalent to the reduction of the vapor layer. However, considering the idea of vapor blockage as a mechanism causing DNB, it would be assumed that for a given subcooling and bulk flow rate, CHF should always occur at the same vapor layer thickness. Comparing these assumptions to the results shown above, where added turbulence increased the CHF, while the vapor layer thickness at CHF decreased resulted in the assumption that the critical parameter is not the thickness of the overall vapor layer, but rather a smaller region closer to the heater. This assumption could be further substantiated by conducting measurements with optical probes. For the time being, the following summary shall be given for effects concerning the bubble crowding mechanism:

1. the 82 % void fraction as criterion for CHF do not appear reasonable, as probe measurements close to the heater have shown much lower void fractions. This has been reported as one of the major weaknesses of the model in a number of reports before (Lee and Mudawar, 1988; Celata et al., 1994; Zhang et al., 2004b).
2. added turbulence reduces the overall vapor layer by a rather constant penetration depth value
3. as this value is constant, relative influence of added turbulence decreases with subcooling as vapor layer thickness increases

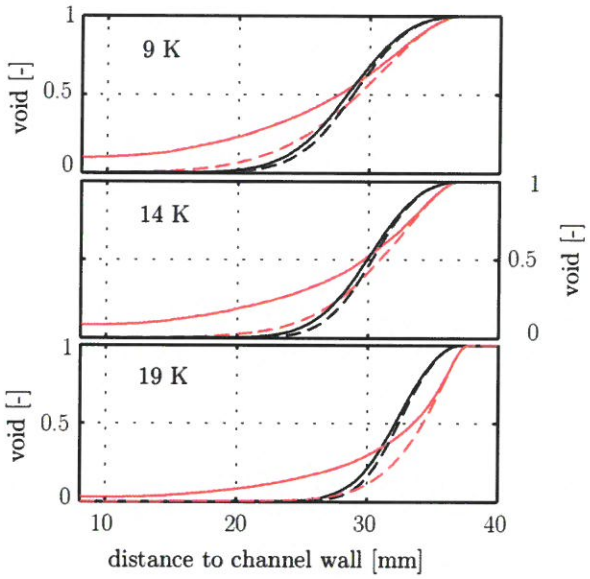

Figure 9. Vapor layer distribution at CHF(-), calculated from high-speed photography (17000 images) for reference case (empty channel, black lines) and case with added turbulence by orifice (red lines) at different subcoolings. Dashed lines indicate values after numerical removal of isolated bubbles. The heater surface is ath the right hand side, at 40 mm.

4. the reduction in overall vapor layer thickness leads to increased access to the relevant bubbly sublayer, increasing CHF by a similar factor as the relative reduction
5. added bulk flow turbulence has less influence on the layer relevant to DNB. This is also evidenced by the constant frequencies of agglomerations for various inserts, subcoolings etc. as shown in (Bloch et al., 2013a).
6. this also suggests that the two-phase enhancement factor used for calculation of the turbulent interchange (see (Weisman and Pei, 1983)) is not correctly formulated as the vapor layer actually blocks bulk flow turbulence, and does not enhance it.
7. the actual trigger parameter does not appear to be the thickness or concentration in the overall vapor layer, but rather an effect in the relevant bubbly sublayer. However, reducing the vapor layer by turbulence (or subcooling) postpones this effect.
8. the use of Prandtl mixing theorem as location of bubbly/bulk interface does not seem appropriate as turbulent interchange is expected to be blocked by a vapor layer before actually reaching the relevant sublayer.
9. finally, a coupling of the model with a viable description of the periodic vapor structure is necessary with the aim of defining the relevant sublayer by analysis of areas of lower vapor concentration.

5.2 Sublayer dryout model: critical evaluation

The mechanisms presented in the sublayer dryout model are generally difficult to investigate experimentally, as the trigger mechanism implies an effect happening in microscopic sublayer that is challenging to access. However, some insight could also be given with the applied techniques. With the used optical probes, measurements up to 0.1 mm distance to the heater surface were possible. The measured void fractions showed no significant change as the probes reached the heater. Therefore, at least in regions of 0.1 mm up to the heater surface, no liquid sublayer could be detected. The equivalent diameter of the vapor cylinders is assumed to be equal to the departure diameter of bubbles under the respective thermal hydraulic conditions, and is expected to stay constant (Lee and Mudawar, 1988). Considering this mechanism, even as the actual liquid sublayer sublayer is not accessible with the available techniques, it should be possible to detect the vapor cylinders close to the heater surface. Figure 10 shows the behavior during CHf at a 9 K subcooling measured with optical probes. In the second plot, the bubble contact time at the probes is given, which represents the bubble size. It could be observed that after passing CHF(+), the contact times at the 2 mm and 4 mm positions started to grow significantly, increasing from a mean value of approx. 2 ms up to 3 ms. At a lower subcooling, the same behavior was also observed for the 6 mm position (Bloch et al., 2013a). This behavior could be interpreted as the forming of larger vapor bubbles or blankets in the direct vicinity of the heater surface. As this behavior directly precedes the abrupt breakdown of the vapor layer (see lower plot) and the associated decrease in heat flux, it can be assumed that the formation of these larger bubbles is actually part of the CHF trigger. Considering the effects reach as far as the second probe at the given subcooling, the bubbles can be expected to stretch at least 2 mm in the radial direction. A rather rough extrapolation of the vapor velocity shown in subsection 4.1 to be at about 1.5 m/s near the heater surface would yield bubble lengths of 4.8 mm for the maximum contact times of 3.2 ms. Comparing this to the critical Helmholtz wavelength as calculated by (Lee and Mudawar, 1988) yields good agreement, with L_m calculated as 4.9 mm for this admittedly rough estimation. It remains somewhat unclear from these measurements how the velocity in the bubbly layer actually develops during the CHF transient. Considering the distinctive velocity gradient towards the heater surface shown above and the increase in bubble size shown here however, it has to be assumed that the velocity increase near the heater is significant. Following the results discussed above for the bubble crowding model, the formation of larger bubbles

shown here fortifies the assumption of relevant effects taking place in a bubbly sublayer close to the heater surface.

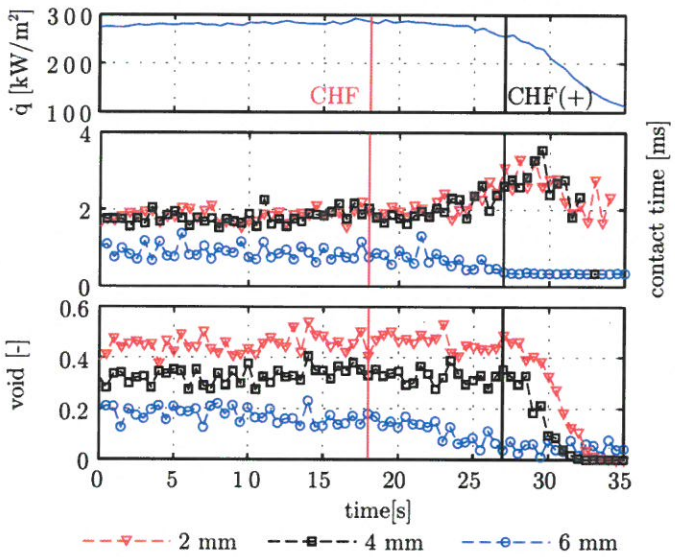

Figure 10. CHF transition behavior: heat flux and bubble size and void fraction from optical probes at different distances to the heater surface (T_{sub}=9 K, v=0.6 m/s).

5.3 Interfacial lift-off model: critical evaluation

As discussed above, in regions close to CHF a significantly periodic behavior of the vapor layer was observed, with self induced acceleration of larger vapor agglomerations leading to a buoyancy controlled flow regime denoted as highly coalesced regime. Such effects were not taken into consideration in the two models discussed above, but form some of the basic assumptions of the interfacial lift-off model. Furthermore, digital holographic interferometry showed that subcooled liquid is present between larger vapor agglomerations (see Figure 7), supporting the assumption of a quenching mechanism relying on the so called wetting fronts, or vapor gaps. Differing observations were made during an analysis of the dynamic behavior of vapor agglomerations. Here, it could be observed from the high speed photography that the shape and structure of the agglomerations hardly remained constant while propagating along the channel. Ongoing coalescence as well as breakup and movement perpendicular to the bulk flow direction led to a constant variation of the agglomerations overall structure. Figure 11 shows photographic images of one vapor agglomeration propagating upwards in the channel over time. Here, the following observations could be made: As agglomerations

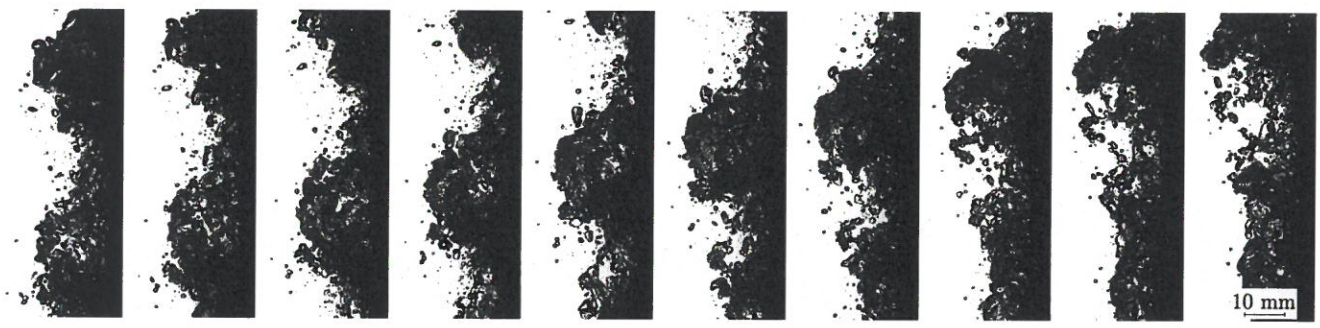

Figure 11. Development of vapor agglomeration over time (subcooling: 9 K, bulk flow velocity: 0.6 m/s, time interval between pictures: 4 ms).

propagate upwards along the channel, vapor from the lower third of the agglomerations is moved towards the heater surface, reducing the size of the overall agglomerations. This could also be interpreted as a larger part of agglomeration being sucked into main vapor layer. This effect can be attributed to the velocity gradient perpendicular to the heater surface, seen as velocity difference between the peaks and the gaps of the agglomerations and also evidenced in the gradient towards the heater surface discussed above. This velocity difference and the associated difference in pressure act as a driving force pulling larger bubbles towards the layer moving at higher velocity. Also, as the agglomerations moved upwards, non coalesced single bubbles were

observed to detach out of the main agglomeration and remain behind, often coalescing into the next agglomeration. These results disagree with the model assumptions given by Galloway and Mudawar (1992) for the description of the wavy vapor layer leading to formulation of the interfacial lift-off model. In the model, a constant vapor layer is assumed at CHF(-), moving at a fixed wave propagation speed. It can be assumed that the narrow channel (depth of 6.4 mm in (Galloway and Mudawar, 1992) and 5 mm in later publications (Gersey and Mudawar, 1995; Sturgis and Mudawar, 1999; Zhang et al., 2004b; Kharangate et al., 2012; Konishi et al., 2013) used in the experiments defining this model does not allow for the formation of a velocity gradient perpendicular to the heated surface, resulting in a rather constant wavy layer. Most likely, the descriptions for the interfacial lift-off can not directly be applied to larger scale channels, as while the general structure may appear similar, the periodic vapor behavior is more strongly governed by buoyancy effects leading to discrepancies with the model assumptions. Using the optical probes, further studies were conducted on the applicability of the interface lift-off as DNB trigger mechanism for the geometry used here. Placing probes at fixed distances of 2, 4 and 6 mm above the heater surface at the trailing edge, following the assumptions of the model, an increase in void fraction at all probe positions would be expected as the interface lifts off shortly prior to CHF. Figure 10 in the previous section shows the results of these measurement at inlet subcoolings of 5 and 27 K. Instead of an increase at all probe positions, at CHF the 6 mm-probe a decrease of void fraction was observed. The other probes however measured an ongoing increase in void fraction, accompanied by an increase in bubble size and frequency (results not shown). This describes a contraction of the vapor layer accompanied by an increase in vapor velocity, rather than a lifting of an otherwise intact wavy interface. These results were also obtained for other subcoolings (Bloch et al., 2013a), with flow inserts and the empty channel and also at higher mass fluxes up to 2000 kg/m^2 s. This leads to the following statements for the interfacial lift-off model:

1. the periodic behavior is taken into consideration, but the model creation in a narrow channel leads to disregard of larger scale coalescence and buoyancy effects as are observed in the channel used here
2. therefore, a velocity gradient and involved acceleration perpendicular to heater surface are observed here that are not described by the interfacial lift-off model
3. the actual trigger mechanism of lift-off was not observed in the experiments
4. rather, a critical drift flux appears to be leading to a critical void fraction in the bubbly sublayer, which finally shuts down turbulent interchange from the bulk

6 Summary

A highly versatile/complementary experimental approach has been presented. The sensibility of the approach could be shown by comparison of the results to available mechanistic models, which provided new insight. A critical comparison of the results to available mechanistic models confirmed some of the assumptions given for the bubble crowding model and the interfacial lift-off model concerning turbulent interchange and vapor behavior respectively. The trigger mechanism proposed for the interfacial lift-off model could not be confirmed in the present results. The bubble crowding mechanism still appears viable, but the result showed a definite need for an expansion of the model to also take coalescence induced effects into consideration. Also, experiments with varying turbulence showed that vapor layer thickness itself is not a viable CHF trigger. It could be shown that nearing CHF, the bubble size also increased considerably in the layer below 4 mm from the heater surface, with a rough estimation confirming the observed bubble sizes to fit the assumptions for the vapor plumes given for the sublayer dryout model. All these points led to the assumption that the actual CHF trigger mechanism can indeed be found in a sublayer close to the heater, as suggested by the bubble crowding and sublayer dryout models. Furthermore, measurements from optical probes, PIV and high-speed photography allowed to give an estimate of drift-flux or slip velocity in the vapor phase towards the heater. It could be concluded that this creates a lift force acting towards the heater surface for larger vapor structures. A new model taking these effects into account appears sensible and shall be presented in more detail in a future report.

REFERENCES

1. Weisman, J.. Letter to the Editor on "Evaluation of Subcooled Critical Heat Flux Correlations for Tubes With and Without Internal Twisted Tapes" by F. Inasaka and H. Nariai and "Consideration of CHF Margin Prediction by Subcooled or Low Quality CHF Ccorrelations" by P. Hejzlar and N.E. Todreas. *Nuclear Engineering and Design* 1996;**163**:259–261.
2. Krepper, E., Rzehak, R.. CFD for Subcooled Flow Boiling: Simulation of DEBORA Experiments. *Nuclear Engineering and Design* 2011;**241**:3851–3866.
3. Lifante, C., Frank, T., Burns, A.. Wall Boiling Modeling Extension Towards the Critical Heat Flux. In: *The 15th International Topical Meeting on Nuclear Reactor Thermalhydraulics, NURETH-15, Pisa, Italy, May 12-15*. 2013, .
4. Weisman, J., Pei, B.S.. Prediction of Critical Heat Flux in Flow Boiling at low Qualities. *Int J Heat Mass Transfer* 1983; **26**:1463–1477.
5. Hebel, W., Detavernier, W., Decreton, M.. A Contribution to the Hydrodynamics of Boiling Crisis in a Forced Flow of Water. *Nuclear Engineering and Design* 1981;**64**:433–445.
6. Hebel, W., Detavernier, W.. On the Velocity Profile of Vapour Bubbles at Critical Heat Flux. *Nuclear Engineering and Design* 1982;**74**:253–257.
7. Ying, S.H., Weisman, J.. Prediction of Critical Heat Flux in Flow Boiling at Intermediate Qualities. *Int J Heat Mass Transfer* 1986;**29**:1639–1648.
8. Lim, J.C., Weisman, J.. A Phenomenologically Based Prediction of the Critical Heat Flux in Channels Containing an Unheated Wall. *Int J Heat Mass Transfer* 1990;**33**:203–205.

9. Yang, J.Y., Weisman, J.. A Phenomenological Model of Subcooled Flow Boiling in the Detached Bubble Region. *International Journal of Multiphase Flow* 1991;**17**:77–94.
10. Lee, C.H., Mudawar, I.. A Mechanistic Critical Heat Flux Model for Subcooled Flow Boiling Based on Local Bulk Flow Conditions. *Int J Multiphase Flow* 1988;**14**:711–728.
11. Haramura, Y., Katto, Y.. A New Hydrodynamic Model of Critical Heat Flux, Applicable Widely to Both Pool and Forced Convection Boiling on Submerged Bodies in Saturated Liquids. *International Journal of Heat and Mass Transfer* 1983;**26**:389–399.
12. Katto, Y.. A Physical Approach to Critical Heat Flux of Subcooled Flow Boiling in Round Tubes. *Int J Heat Mass Transfer* 1990a; **33**:611–620.
13. Katto, Y.. Prediction of Critical Heat Flux of Subcooled Flow Boiling in Round Tubes. *Int J Heat Mass Transfer* 1990b;**33**:1921–1928.
14. Celata, G.P., Cumo, M., Mariani, A., Simoncini, M., Zummo, G.. Rationalization of Existing Mechanistic Models for the Prediction of Water Subcooled Flow Boiling Critical Heat Flux. *Int J Heat Mass Transfer* 1994;**37**:347–360.
15. Celata, G.P., Cumo, M., d´Annibale, F.. Direct Contact Evaporation of Nearly Saturated R 114 in Water. *Int J Heat Mass Transfer* 1995;**38**:1495–1504.
16. Celata, G.P., Cumo, M., Katto, Y., Mariani, A.. Prediction of the Critical Heat Flux in Water Subcooled Flow Boiling Using a new Mechanistic Approach. *International Journal of Heat and Mass Transfer* 1999;**42**:1457–1466.
17. Mudawwar, I., Incropera, T., Incropera, F.. Boiling Heat Transfer and Critical Heat Flux in Liquid Film Falling on Vertically-Mounted Heat Sources. *International Journal of Heat and Mass Transfer* 1987;**30**:2083–2095.
18. Galloway, J., Mudawar, I.. CHF Mechanism in Flow Boiling From a Short Heated Wall - I. Examination of Near-Wall Conditions With the aid of Photomicrography and High-Speed Video Imaging. *Int J Heat Mass Transfer* 1993a;**36**:2511–2526.
19. Galloway, J., Mudawar, I.. CHF Mechanism in Flow Boiling From a Short Heated Wall - II. Theoretical CHF Model. *Int J Heat Mass Transfer* 1993b;**36**:2527–2540.
20. Zhang, H., Mudawar, I., Hasan, M.M.. Experimental Assessment of the Effects of Body Force, Surface Tension Force, and Inertia on Fow Boiling CHF. *International Journal of Heat and Mass Transfer* 2002;**45**:4079–4095.
21. Zhang, H., Mudawar, I., Hasan, M.M.. A Method for Assessing the Importance of Body Force on Flow Boiling CHF. *Journal of Heat Transfer* 2004a;**126**:161–168.
22. Konishi, C., Mudawar, I., Hasan, M.M.. Investigation of Localized Dryout Versus CHF in Saturated Fow Boiling. *International Journal of Heat and Mass Transfer* 2013;**67**:131–146.
23. Tong, L., Weisman, J.. *Thermal Analysis of Pressurized Water Reactors, 3rd ed.* American Nuclear Society, La Grange Park, Illinois; 1996.
24. Bloch, G., Kuczaty, J., Sattelmayer, T.. Application of high-speed digital holographic interferometry for the analysis of temperature distributions and velocity fields in subcooled flow boiling. *Experiments in Fluids* 2014;**55**(2):1–12.
25. Bloch, G., Jochum, C., Schechtl, T., Sattelmayer, T.. Subcooled Flow Boiling in a Rectangular Channel With Added Turbulence and Longitudinal Vortices. In: *Proceedings of the 2012 20th International Conference on Nuclear Engineering collocated with the ASME 2012 Power Conference*. Anaheim, USA; 2012, .
26. Bloch, G., Sattelmayer, T.. Effects of turbulence and secondary flows on subcooled flow boiling. *Heat and Mass Transfer* 2014; **50**(3):427–435.
27. Bloch, G., Muselmann, W., Saier, M., Sattelmayer, T.. A Phenomenological Study on Effects Leading to the Departure From Nucleate Boiling in Subcooled Flow Boiling. *International Journal of Heat and Mass Transfer* 2013a;**67**:61–69.
28. Bloch, G., Elfner, J., Finke, K., Sattelmayer, T.. Setup and Fabrication of Cost Effective, Robust Fiber Optical Needle Probes for Application in Multiphase Flows. In: *Lasermethoden in der Strömungsmesstechnik*. München, Germany; 2013b, .
29. Bang, C., Chang, S.H., Baek, W.P.. Visualization of the Subcooled Fow Boiling of R-134a in a Vertical Rectangular Channel With an Electrically Heated Wall. *International Journal of Heat and Mass Transfer* 2004;**47**:4349–4363.
30. Jiji, L.M.. *Incipient boiling and the Bubble Boundary Layer Formation Over a Heated Plate for Forced Convection Flow in a Pressurized Rectangular Channel*. Ph.D. thesis; University of Michigan; 1962.
31. Zhang, H., Mudawar, I., Hasan, M.M.. Investigation of Interfacial Behavior During the Flow Boiling CHF Transient. *International Journal of Heat and Mass Transfer* 2004b;**47**:1275–1288.
32. Galloway, J.E., Mudawar, I.. Critical Heat Flux Enhancement by Means of Liquid Subcooling and Centrifugal Force Induced by Flow Curvature. *Int J Heat Mass Transfer* 1992;**35**:1247–1260.
33. Gersey, C.O., Mudawar, I.. Effects of Heater Length and Orientation on the Trigger Mechanism for Near-Saturated Flow Boiling Critical Heat Flux - II. Critical Heat Flux Model. *Int J Heat Mass Transfer* 1995;**38**:643–654.
34. Sturgis, J.C., Mudawar, I.. Critical Heat Flux in a Long, Rectangular Channel Subjected to One-Sided Heating - I. Flow Visualization. *International Journal of Heat and Mass Transfer* 1999;**42**:1835–1847.
35. Kharangate, C.R., Mudawar, I., Hasan, M.M.. Photographic Study and Modeling of Critical Heat Flux in Horizontal Flow Boiling with Inlet Vapor Void. *International Journal of Heat and Mass Transfer* 2012;**55, Issues 15-16**:4154–4168.